An aggregate model for transient and multi-directional pedestrian flows in public walking areas

Flurin S. Hänseler* Michel Bierlaire* Bilal Farooq†
Thomas Mühlematter*

December 19, 2013

Report TRANSP-OR 131219
Transport and Mobility Laboratory
School of Architecture, Civil and Environmental Engineering
Ecole Polytechnique Fédérale de Lausanne
transp-or.epfl.ch

*École Polytechnique Fédérale de Lausanne (EPFL), School of Architecture, Civil and Environmental Engineering (ENAC), Transport and Mobility Laboratory, Switzerland, {flurin.haenseler,michel.bierlaire,thomas.muhlematter}@epfl.ch

†Département des Génies Civil, Géologique et des Mines, Polytechnique Montréal, Canada, bilal.farooq@polymtl.ca

Abstract

A dynamic pedestrian propagation model applicable to congested and multi-directional flows is proposed. Based on the cell transmission model, several important extensions are made to describe the simultaneous and potentially conflicting propagation of multiple pedestrian groups. Their movement across space and time can be individually tracked, such that group-specific travel time distributions can be predicted. Cell potentials allow for en-route path choice that takes into account prevailing traffic conditions. The model is formulated at the aggregate level and thus computationally cheap, which is advantageous for studying large-scale problems. A detailed analysis of several basic flow patterns including counter- and cross flows, as well as two generic scenarios involving a corner- and a bottleneck flow is carried out. Depending on the choice of model parameters, various behavioral patterns ranging from disciplined queueing to impatient jostling can be realistically reproduced. Following a systematic model calibration using real data, an extensive case study involving a Swiss railway station is presented. A comparison with the social force model and pedestrian tracking data shows a good performance of the proposed model with respect to predictions of travel times and pedestrian density fields.

Keywords: Pedestrian propagation, cell-transmission model, multi-directional flow, en-route path choice, calibration.

1 Introduction

In railway stations and other public spaces, pedestrian flows are often multi-directional, non-stationary and congested (Daamen, 2004). To gain a better understanding of such flows, there is a general need for adequate, quantitative models that can predict pedestrian movements and travel times for a given infrastructure and demand.

A central challenge in pedestrian flow modeling consists in predicting level of service (LOS) of walking facilities. From a modeling point of view, LOS assessment requires the assignment of pedestrian demand to the infrastructure and the computation of resulting flows. In this process, the number of pedestrians traveling between each origin-destination pair needs to be known a priori. Local flows are calculated by a pedestrian propagation model, from which various LOS indicators can be extracted. A typical LOS indicator is for instance pedestrian density, which is considered an important factor for safety and customer satisfaction.

A recent review of pedestrian propagation models has been carried out by Duives et al. (2013), who provide a broad overview of modeling achievements in the last two decades. Their study covers in particular the social force model (Helbing and Molnár, 1995), cellular automata (Blue and Adler, 2001), queueing networks (Løvås, 1994), behavioral models (Robin et al., 2009), activity choice models (Hoogendoorn and Bovy, 2004), continuum models (Hughes, 2002) and two further models that are associated with the gaming industry. These models are compared and evaluated with respect to three criteria. First, their ability to reproduce basic movement patterns such as a bottleneck- or a bi-directional flow is assessed. Second, their capabilities to describe self-organization phenomena such as lane formation or stop-and-go waves is examined. Third, practical considerations such as computational cost and general applicability are investigated.

One of the conclusions of their study is that current models can be divided into slow but precise microscopic approaches and fast but behaviorally questionable macroscopic modeling attempts. It is argued that for crowd simulation models to be used in practice, the identified gap needs to be closed. This is where the present study would like to make a contribution. Our approach does not fit in any of the model categories listed by Duives et al. (2013). It is designed such that it is not only useful for infrastructure assessment, but also helpful in the inverse problem of estimating

pedestrian demand.

In transportation hubs, pedestrian demand changes rapidly and may fluctuate by several orders of magnitude over a day. Both the total number of pedestrian trips per time and the corresponding route fractions may continuously change. A precise demand estimation requires thus the combination of several information sources such as pedestrian flow counters, pedestrian tracking systems or sales data from service points and ticket vending machines. To associate sensor data obtained at different locations over space and time, it is crucial to have an accurate estimate of walking times.

The above modeling problems – infrastructure assessment, flow assignment, demand estimation – are closely interwoven. Flow propagation depends on demand. Inversely, demand estimation relies on travel time predictions provided by a pedestrian propagation model. In this work, we focus on a flow propagation model, but keep these interdependencies in mind. Specifically, we aim at developing a pedestrian propagation model that can accurately predict travel time distributions, flows and pedestrian densities, and is versatile enough to interact with a demand estimation and an assignment model.

For this purpose, we propose the use of an aggregate pedestrian flow model due to several reasons: First, aggregate models are computationally cheap and can therefore be readily integrated in a dynamic pedestrian traffic assignment model (in the context of car traffic e.g. Ben-Akiva et al., 2001; Mahmassani, 2001; Abdelghany et al., 2012). Such a joint demand estimation/flow assignment approach typically requires solving a fixed point (see Bierlaire and Crittin, 2006; Cascetta and Postorino, 2001, for related examples). This makes multiple runs of the pedestrian propagation model necessary, amplifying the performance difference between aggregate and disaggregate models. In such a context, the use of disaggregate models for large problems would quickly become infeasible. Second, the problem of origin-destination demand estimation is often considered at the aggregate level (again examples from car traffic: Cascetta et al., 1993; Ashok and Ben-Akiva, 2000; Sherali and Park, 2001). In this case, an assignment model operating at the same level of aggregation allows for direct interaction with the demand estimation methodology without prior population synthesis, which is computationally advantageous. Third, calibration of macroscopic models is relatively easy (Hoogendoorn and Bovy, 2001). In

contrast, calibration of microscopic models is challenging due to various reasons. Often a lack of disaggregate data necessitates a calibration based on a comparison of macroscopic outcomes of the model. Such an approach is unlikely to produce the optimal parameters since the number of degrees of freedom is too large. It is not guaranteed that the obtained specification is able to describe individual behavior accurately, or if it merely provides a reasonable average macroscopic prediction for the situation it is calibrated for (Hoogendoorn and Daamen, 2007). If disaggregate data is available, calibration still remains difficult. For the widely used social force model, microscopic calibration has been achieved only for a controlled bottleneck flow (Hoogendoorn and Daamen, 2007), or by neglecting inter-pedestrian variability (Johansson et al., 2007).

In the following, we first give an overview of existing aggregate pedestrian propagation models. We then outline a new model, explicitly designed for dynamic, multi-directional and congested pedestrian flow problems. Subsequently, this model is calibrated on real data, analyzed in detail using various test cases, and applied to a case study.

2 Aggregate pedestrian flow models

In the literature, three types of aggregate pedestrian propagation models have been considered: (i) Models based on continuum theory for pedestrian flows, (ii) queueing network based models (QNM), and (iii) cell transmission models (CTM).

The first type is aggregate with respect to agents, and operates in continuous space. The second type considers pedestrians at the disaggregate level, relying on a graph-based space representation. The third model type is aggregate both with respect to space and pedestrians, i.e., space is 'aggregated' to a network, and pedestrians are subsumed as groups.

Continuum theory for pedestrians is formulated as a set of partial differential equations, in which the direction of flow is defined by one or several continuous potential fields (Hughes, 2002). It is mostly used for evacuation simulations, where only a small number of origin-destination flows need to be considered.

QNM is based on random queueing processes and can be either approximated analytically for stationary problems (Cheah and Smith, 1994;

Osorio and Bierlaire, 2009), or by simulation (Løvås, 1994; Daamen, 2004; Rahman et al., 2013). Propagation of agents along their route is described at the disaggregate level. Due to the microscopic nature of QNM, it is straightforward to consider agent-specific routes. In the context of car traffic, Çetın (2005) reports that an accurate modeling of backward traveling jam waves using QNM is difficult. Guaranteeing a fair behavior in 'intersections' seems possible, but is far from trivial (Charypar, 2008, again in the context of car traffic).

CTM represents a finite difference approximation to first-order flow theory (Daganzo, 1994, 1995). Like the continuum theory for pedestrians, it represents a deterministic approach and is of aggregate nature, which makes it computationally cheap. For prediction of flows, CTM relies on a fundamental diagram relating density and speed.

A few studies consider CTM or derived concepts to study pedestrian flows. Al-Gadhi and Mahmassani (1991) developed a cell-based pedestrian walking model with application to the circular movements around stone monuments occurring during the Hajj, a Muslim pilgrimage to Makkah, Saudi Arabia. The model consists of a set of coupled differential equations including a flow conservation equation that is solved numerically. A speed-density relationship is considered to describe the multidirectional movement. Their work can be seen as an early prototype of the CTM introduced later by Daganzo. Asano et al. (2007) extended CTM to describe general multi-directional pedestrian flows, assuming a trapezoidal fundamental diagram inherited from the original CTM. Their model is applicable to cases where the exact sequence of cells that a pedestrian traverses is known in advance. They illustrate the model using a generic cross-flow problem. Guo et al. (2011) developed a cell-based model for describing evacuation processes. Instead of relying on a density-flow relationship, they assume that the number of pedestrians exchanged between adjacent cells depends on the 'opening' between them. The size of this opening is given exogenously, which represents a major simplification with respect to the original CTM. Flows between cells are computed based on cell potentials, cell capacity constraints and the previously mentioned openings. Besides the cell-based space representation, their model is not directly related to Daganzo's CTM and hardly applicable to other problems than evacuation.

In this study, we develop an aggregate pedestrian propagation model based on the original CTM and the above mentioned derived models.

Thanks to the use of an empirical fundamental diagram for pedestrian flows, it can realistically reproduce pedestrian flow patterns under many conditions. In particular, this includes pedestrian waves, which often occur in transportation hubs after the arrival of mass transport vehicles such as trains. We build on the framework for multi-directional flows proposed by Asano et al. (2007) and adapt the concept of cell-specific potentials proposed by Guo et al. (2011). This approach allows for en-route path choice, making an exogenous definition of exact cell sequences for pedestrians needless. The resulting model can accurately describe everyday pedestrian flows in public walking areas and is performant thanks to its aggregate nature.

3 A cell-based pedestrian flow model

The cell transmission model considers time in discrete space, i.e., the period of analysis is discretized into a set of intervals $\mathcal{T}$, where each interval $\tau = 1, \ldots, T$ is of uniform length Δt. Similarly, space is discretized into square cells ξ of characteristic length ΔL as shown in figure 1. In principle, triangular or hexagonal grids are possible as well, but most practical layouts can be represented more realistically with a square grid that inherently allows for orthogonal movements.

The cell network is represented by a directed graph $\mathcal{G} = (\mathcal{X}, \mathcal{Y})$, where $\mathcal{X}$ represents the set of cells ξ and $\mathcal{Y}$ the set of links $\xi \to \xi'$ connecting them. Each cell has an individual area A_ξ, which may deviate from the default size ΔL^2 in presence of obstacles. Such obstacles include any object that reduces the walkable space in a cell but is small in comparison, such as e.g. a pillar or a trash bin. Adjacent cells are connected to each other if they share a cell edge. The set of neighbors of a cell ξ is denoted by $\mathcal{N}_\xi$. Pedestrian flows from one cell to another are governed by the flow propagation model described in the following.

The central idea of the cell transmission model is to formulate a conservation principle with respect to the number of pedestrians in each cell and to combine it with a fundamental diagram for calculating the flows between them. Within a cell, pedestrians are assumed to be homogeneously distributed, and their movements are not modeled explicitly.

To estimate the walking speed of pedestrians, an empirical density-speed relation is employed. Let k denote the space-mean density, i.e., the number

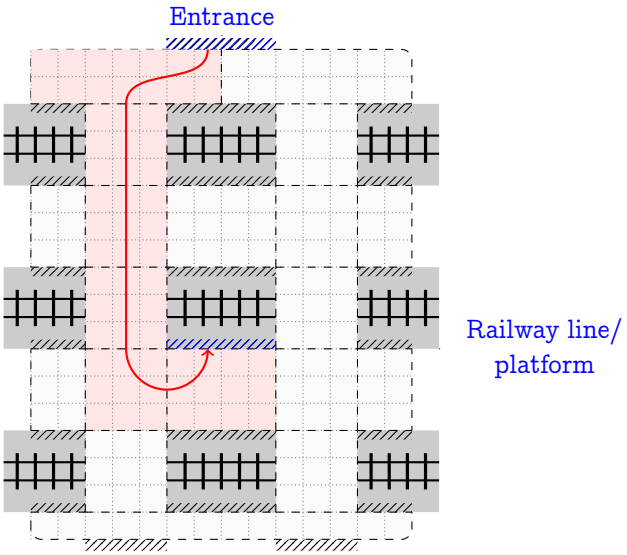

Figure 1: Space is discretized into a number of cells (delimited by dotted lines). Contiguous sets of cells represent areas (delimited by dashed lines). Each pedestrian is assigned to a sequence of these areas, which is referred to as a route (example shown in red).

of pedestrians per unit space, and let v be the space-mean speed, defined as the average speed of pedestrians per unit space. According to Weidmann (1993), the velocity of pedestrians in public spaces depends on density as follows (figure 2)

$$v(k) = v_f \left\{ 1 - \exp\left[-\gamma \left(\frac{1}{k} - \frac{1}{k_c} \right) \right] \right\}, 0 \leq k \leq k_c, \tag{1}$$

where v_f denotes free-flow speed (1.34 m/s according to Weidmann, 1993), γ is a shape parameter (1.913 m^{-2}), and k_c represents jam density (5.4 m^{-2}). Being one of the most widely used empirical fundamental diagrams, we utilize it in this work as well. Generalizations to other fundamental diagrams turn out to be straightforward. Common to all of them is that they do not consider speed as a vector, but as a scalar representing some average value. An overview of existing pedestrian fundamental diagrams is provided e.g. by Seyfried et al. (2005).

To guarantee the equivalence between CTM and kinematic wave theory, the time step Δt has to be chosen in agreement with the free-flow speed v_f and the cell length ΔL. Specifically, the following relation has to be fulfilled

$$v_f \Delta t = \Delta L, \tag{2}$$

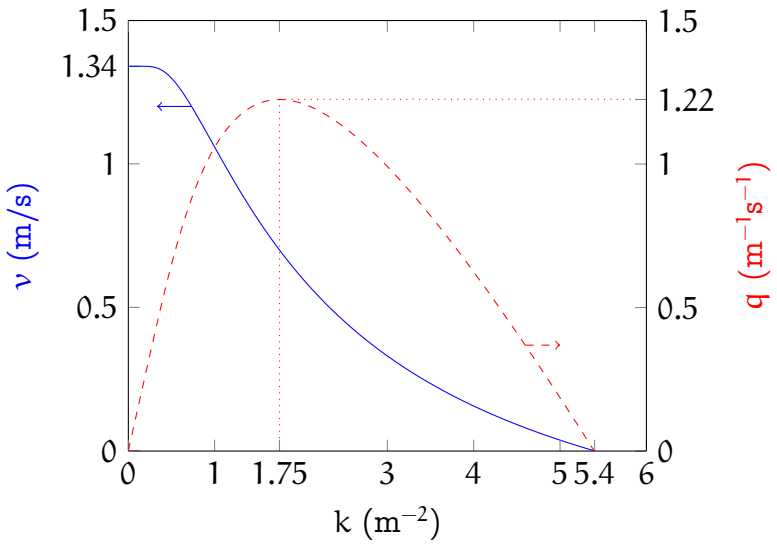

Figure 2: Pedestrian space-mean speed (solid blue) and specific hydrodynamic flow (dashed red) as a function of density according to Weidmann (1993).

which implies that under free-flow conditions, pedestrians propagate from one cell to the next during one time step. A derivation of this condition is provided by Daganzo (1994).

For pedestrians within a given cell, the edge through which they enter and leave the cell are known. We assume that they cross these edges orthogonally. The sum of all pedestrians in the cell, $N = k\Delta L^2$, can be attributed to the contributions of each pair of inflow and outflow edge $\{i, j\}$, $N_{i,j}$, such that $N = \sum_{i=1}^{4} \sum_{j=1}^{4} N_{i,j}$.

The cumulated outflow across edge $j \in \{1, 2, 3, 4\}$ during an infinitesimal time interval dt associated with the fundamental diagram is then equal to the number of pedestrians in an infinitesimal area of size $\Delta L v(k) dt$ that are headed to edge j, i.e.,

$$dQ_j^{out} = \Delta L v(k) dt \sum_{i=1}^{4} \frac{N_{i,j}}{\Delta L^2}, \tag{3}$$

where the unit is number of pedestrians. By taking the sum over all edges, the cumulated outflow from a cell during an infinitesimal time interval dt

associated with the fundamental diagram is given by

$$dQ_{tot}^{out} = \Delta L v(k) dt \sum_{i=1}^{4} \sum_{j=1}^{4} \frac{N_{i,j}}{\Delta L^2} = \Delta L v(k) dt k. \tag{4}$$

Dividing by the cell length ΔL and the infinitesimal time interval dt, the specific outflow from a cell associated with the fundamental diagram can be obtained (figure 2)

$$q_h(k) = v(k)k. \tag{5}$$

Equation 5 is referred to as hydrodynamic flow-density relation in the literature (see e.g. Kesting, 2012, for an example in the context of multi-lane car traffic). The quantity q_h, which is a function of the overall density k only, is accordingly referred to as hydrodynamic flow.

Previously, $q_h(k)$ has been derived based on the outflow from a cell. The same expression results if the derivation is based on the inflow. The hydrodynamic flow $q_h(k)$ represents a characteristic flow per unit time and unit length that is associated with the density-speed relation (1). Since it only considers the density of a single cell, and since it does not take into account any capacity constraints that will be discussed in the following, it does not represent an actual flow.

Let us now introduce a concept allowing to describe how pedestrians interact with their environment. We assume that there exists a finite set of routes $\mathcal{R}$ along which pedestrians can walk. Intuitively, a route $\rho \in \mathcal{R}$ can be thought of as a sequence of areas without loops, $\rho = (r_o^\rho, r_1^\rho, r_2^\rho, \ldots, r_d^\rho)$, such as 'entrance north, train station hall, pedestrian underpass west, platform #3'. Each of these areas r represents a non-empty subgraph of $\mathcal{G}$. The first and the last area, r_o and r_d, consist of exactly one cell. These boundary cells can be adjacent to an arbitrary number of cells and are not subject to any capacity constraints. While their typical position is at the border of a walking area, boundary cells can also be located in the interior if they represent an access way to e.g. an elevator or an escalator. There can be several routes connecting the same pair of boundary cells. Each route starts and ends at a boundary cell, but cannot contain a boundary cell in between.

Pedestrian demand along a route $\rho \in \mathcal{R}$ emanating during time interval τ is denoted by $X_{\rho,\tau}$. A pedestrian group ℓ is defined by a route ρ_ℓ and a departure time interval τ_ℓ. Group size $X_{\rho,\tau}$ is its main characteristic.

Several groups can share the same route ρ if they are assigned to a different departure time interval and vice versa. The set of all pedestrian groups is denoted by $\mathcal{L} \subset \mathcal{R} \times \mathcal{T}$. In this work, we assume that the pedestrian route demand $\mathbf{X} = [X_{\rho,\tau}]$ is known a priori.

To apply the density-speed relation (1) to a cell, we need to know its occupation. The total population in cell ξ during time interval τ is given by

$$M(\xi, \tau) = \sum_{\ell \in \mathcal{L}} M_\ell(\xi, \tau) \tag{6}$$

where $M_\ell(\xi, \tau)$ represents the number of people in cell ξ during interval τ that belong to group ℓ. The cumulated hydrodynamic flow of cell ξ during time interval τ, formally defined as the integral of hydrodynamic flow (equation 5) over the interval τ and the circumference of cell ξ, reads for Weidmann's fundamental diagram (equation 1) as

$$Q_\xi(\tau) = M(\xi, \tau) \left\{ 1 - \exp\left[-\gamma A_\xi \left(\frac{1}{M(\xi, \tau)} - \frac{1}{N_\xi} \right) \right] \right\} \tag{7}$$

where $N_\xi = k_c A_\xi$ denotes the maximum number of people that can be contained by cell ξ at jam density k_c. The cumulated hydrodynamic cell flow reaches a cell-specific optimum $Q_{\xi,\mathrm{opt}}$ at occupation $M_{\xi,\mathrm{opt}}$, similar to the hydrodynamic flow shown in figure 2. Two quantities are derived from it: The hydrodynamic outflow capacity denotes the maximum number of pedestrians that can leave cell ξ during time interval τ according to the fundamental diagram, and is given by

$$\tilde{Q}_\xi(\tau) = \begin{cases} Q_\xi(\tau) & \text{if } M(\xi, \tau) \leq M_{\xi,\mathrm{opt}}, \\ Q_{\xi,\mathrm{opt}} & \text{otherwise.} \end{cases} \tag{8}$$

Similarly, the hydrodynamic inflow capacity represents the maximum number of people that can enter cell ξ during time interval τ according to the fundamental diagram and is defined as

$$\hat{Q}_\xi(\tau) = \begin{cases} Q_{\xi,\mathrm{opt}} & \text{if } M(\xi, \tau) \leq M_{\xi,\mathrm{opt}}, \\ Q_\xi(\tau) & \text{otherwise.} \end{cases} \tag{9}$$

For en-route path choice, a static floor field F_ξ^ρ and a dynamic floor field $H_\xi(\tau)$ are introduced. The route-specific static floor field F_ξ^ρ represents the remaining distance from cell ξ along route ρ, i.e., the minimum number

of cells to be traversed from cell ξ to the end of route ρ along route ρ. It can be calculated using any shortest path algorithm (e.g. Dijkstra, 1959). The dynamic floor field $H_\xi(\tau)$ is assumed to be equal to the prevailing normalized walking speed $v\left(M(\xi,\tau)/A_\xi\right)/v_f$. The rationale behind this choice is that pedestrians are expected to give preference to cells in which they can walk at free-flow speed, similar to the concept of the desired velocity in the social force model (Helbing and Molnár, 1995).

Based on these floor fields, each cell is assigned a route-specific, density-dependent potential

$$P_\xi^\rho(\tau) = \alpha F_\xi^\rho - \beta H_\xi(\tau) \tag{10}$$

where the parameters $\alpha, \beta \in \mathbb{R}^+$ denote weights that can assume any positive value and do not need to sum up to unity. Both floor fields as well as the corresponding weights are non-dimensional.

From the cell potentials, turning proportions for local path choice can be calculated. Pedestrians can only be sent to adjacent cells that are part of their route. The set Θ_ξ^ρ contains all cells which are adjacent to cell ξ and part of route ρ. Assuming that all pedestrians embarked on a given route have the same behavior, the turning proportion corresponding to link $\xi \rightarrow \vartheta \in \Theta_\xi^\rho$ for the ensemble of people following route ρ that are in cell ξ during time interval τ can be expressed as

$$\delta_{\xi\rightarrow\vartheta}^\rho(\tau) = \frac{\exp\left\{P_\xi^\rho(\tau) - P_\vartheta^\rho(\tau)\right\}}{\sum_{\vartheta' \in \Theta_\xi^\rho} \exp\left\{P_\xi^\rho(\tau) - P_{\vartheta'}^\rho(\tau)\right\}}. \tag{11}$$

Expression 11 is consistent with the discrete choice theory (Ben-Akiva and Lerman, 1985), according to which it represents the probability of a single agent in cell ξ embarked on route ρ to be headed to cell $\vartheta \in \Theta_\xi^\rho$ during time interval τ. Due to the assumption of a homogeneous population, it also represents the turning proportion of the ensemble of pedestrians traveling on the same route. The use of a more advanced model (?Robin et al., 2009) could be considered. However, there is a trade-off between behavioral realism and computational performance which should be assessed first.

The combination of equations (10) and (11) provides a behavioral interpretation of the weights α and β. A large value of α means that pedestrians follow the shortest path corresponding to their route very closely. Analogically, a high value of β implies that pedestrians prefer less busy cells in which they can walk as fast as possible.

As in the original cell transmission model proposed by Daganzo (1995), a sending and receiving capacity is defined for each cell, representing the maximum number of pedestrians who can leave and enter a cell, respectively.

The sending capacity of cell ξ to cell $\vartheta \in \Theta_\xi^\rho$ for group ℓ during time interval τ is given by

$$S_{\xi\to\vartheta}^{\ell}(\tau) = \delta_{\xi\to\vartheta}^{\rho_\ell}(\tau) \min\left\{ M_\ell(\xi,\tau), \frac{M_\ell(\xi,\tau)}{M(\xi,\tau)} \tilde{Q}_\xi(\tau) \right\}. \tag{12}$$

Under non-congested conditions, all pedestrians advance to the next cell (first term in curly brackets). In the presence of congestion, i.e., if the sum of pedestrians in cell ξ is superior to the hydrodynamic outflow capacity $\tilde{Q}_\xi(\tau)$, the latter is assigned to all groups present in cell ξ according to a demand-proportional supply distribution scheme (Asano et al., 2007).

The counterpart of the sending capacity is the receiving capacity. For cell ξ and time interval τ, it can be expressed as

$$R_\xi(\tau) = \min\left\{ N_\xi - M(\xi,\tau), \hat{Q}_\xi(\tau) \right\} \tag{13}$$

where the first term in brackets represents the number of pedestrians for which space is left in the cell, and the second term represents the hydrodynamic inflow capacity.

The actual flow of people belonging to group ℓ from cell ξ to an adjacent cell $\vartheta \in \Theta_\xi^{\rho_\ell}$ during time interval τ can be expressed as

$$Y_{\xi\to\vartheta}^{\ell}(\tau) = \begin{cases} S_{\xi\to\vartheta}^{\ell}(\tau) & \text{if } \sum_{\nu\in\mathcal{N}_\vartheta} \sum_{\ell\in\mathcal{L}} S_{\nu\to\vartheta}^{\ell}(\tau) \le R_\vartheta(\tau), \\ \zeta_{\xi\to\vartheta}^{\ell}(\tau) R_\vartheta(\tau) & \text{otherwise.} \end{cases} \tag{14}$$

In the presence of congestion, i.e., if the sum of sending capacities allocated to a cell exceeds the receiving capacity of that cell, it is allocated proportionally to the various inflowing groups (Asano et al., 2007). The supply distribution scheme for the receiving capacity is then given by

$$\zeta_{\xi\to\vartheta}^{\ell}(\tau) = \frac{S_{\xi\to\vartheta}^{\ell}(\tau)}{\sum_{\nu\in\mathcal{N}_\vartheta} \sum_{\ell\in\mathcal{L}} S_{\nu\to\vartheta}^{\ell}(\tau)}. \tag{15}$$

Note that flows to cells which are not adjacent with respect to the route of interest are always zero, i.e., $Y_{\xi\to\vartheta'}^{\ell}(\tau) = 0$ if $\vartheta' \notin \Theta_\xi^{\rho_\ell}$.

For boundary cells, an exogenous generation term $W_\ell(\xi,\tau)$ adds outgoing groups at their origin during the foreseen departure time interval, and removes incoming groups arriving at their destination

$$W_\ell(\xi,\tau) = \begin{cases} X_{\rho_\ell,\tau_\ell} & \text{if } \xi \in r_o^{\rho_\ell},\ \tau = \tau_\ell, \\ -M_\ell(\xi,\tau) & \text{if } \xi \in r_d^{\rho_\ell}, \\ 0 & \text{otherwise.} \end{cases} \tag{16}$$

This term is different from zero only for boundary cells.

Once inter-cell flows and generation terms are known, a flow balance equation allows to calculate the occupation of group ℓ in cell ξ during time interval τ

$$M_\ell(\xi,\tau+1) = M_\ell(\xi,\tau) + \sum_{\nu\in\mathcal{N}_\xi} \left(Y^\ell_{\nu\to\xi}(\tau) - Y^\ell_{\xi\to\nu}(\tau)\right) + W_\ell(\xi,\tau). \tag{17}$$

Iteratively applying the above recursion scheme to all groups $\ell \in \mathcal{L}$ and cells $\xi \in \mathcal{X}$ allows to calculate the propagation of pedestrians during the complete time horizon $\mathcal{T}$ provided that the demand $\mathbf{X}$ and the initial state of the system are known. The model is independent of the processing order, i.e., the order in which cells are updated does not have an influence on the dynamics of the model. In the following, recursion (17) and the corresponding set of equations is referred to as *pedestrian cell transmission model* (PedCTM).

PedCTM possesses a set of five parameters $Z = (v_f, \gamma, k_c, \alpha, \beta)$. By means of a coordinate transformation shown in the following, it can be reduced to three. Let $N = \Delta L^2 k_c$ denote the maximum number of pedestrians that a standard cell can accommodate at the jam density, $a_\xi = A_\xi/\Delta L^2$ the normalized area of cell ξ, and let $\omega = \gamma/k_c$ represent the ratio of the shape parameter γ and the critical density k_c. The normalized PedCTM can then be expressed as

$$\begin{aligned} m(\xi,\tau) = \quad M(\xi,\tau)/N \quad &= \sum_{\ell\in\mathcal{L}} m_\ell(\xi,\tau), \\ q_\xi(\tau) = \quad Q_\xi(\tau)/N \quad &= m(\xi,\tau)\left\{1 - \exp\left[-\omega\left(\frac{a_\xi}{m(\xi,\tau)} - 1\right)\right]\right\}, \\ s^\ell_{\xi\to\vartheta}(\tau) = \quad S^\ell_{\xi\to\vartheta}(\tau)/N \quad &= \delta^{\rho_\ell}_{\xi\to\vartheta}(\tau)\min\left\{m_\ell(\xi,\tau), \frac{m_\ell(\xi,\tau)}{m(\xi,\tau)}\tilde{q}_\xi(\tau)\right\}, \\ r_\xi(\tau) = \quad R_\xi(\tau)/N \quad &= \min\{a_\xi - m(\xi,\tau), \hat{q}_\xi(\tau)\}, \end{aligned} \tag{18}$$

$$
\begin{aligned}
y^{\ell}_{\xi\to\vartheta}(\tau) = \quad Y^{\ell}_{\xi\to\vartheta}(\tau)/N \quad &= \begin{cases} s^{\ell}_{\xi\to\vartheta}(\tau) & \text{if } \sum_{\nu\in\mathcal{N}_\vartheta}\sum_{\ell\in\mathcal{L}} s^{\ell}_{\nu\to\vartheta}(\tau) \le r_\vartheta(\tau), \\ \zeta^{\ell}_{\xi\to\vartheta}(\tau) r_\vartheta(\tau) & \text{otherwise,} \end{cases} \\
w_\ell(\xi,\tau) = \quad W_\ell(\xi,\tau)/N \quad &= \begin{cases} x_{\rho_\ell,\tau_\ell} & \text{if } \xi \in r_o^{\rho_\ell},\ \tau = \tau_\ell, \\ -m_\ell(\xi,\tau) & \text{if } \xi \in r_d^{\rho_\ell}, \\ 0 & \text{otherwise,} \end{cases} \\
m_\ell(\xi,\tau+1) = \quad M_\ell(\xi,\tau)/N \quad &= m_\ell(\xi,\tau) + \sum_{\nu\in\mathcal{N}_\xi} \left(y^{\ell}_{\nu\to\xi}(\tau) - y^{\ell}_{\xi\to\nu}(\tau) \right) + w_\ell(\xi,\tau).
\end{aligned}
$$

This set of equations allows to compute the normalized occupation $m_\ell(\xi,\tau)$ for all groups, cells, time intervals from normalized demand $\mathbf{x} = \mathbf{X}/N$ (with $x_{\rho,\tau} = X_{\rho,\tau}/N$) as a function of the dimensionless parameters α, β and ω.

Like for α and β, a behavioral interpretation can be found for the parameter ω as well. Figure 3 shows the normalized hydrodynamic cell flow (equation 18) as a function of cell occupation for different values of ω. The solid curve in red corresponds to a value of $\omega = 0.354$ obtained for Weidmann's specification of the pedestrian fundamental diagram (Weidmann, 1993).

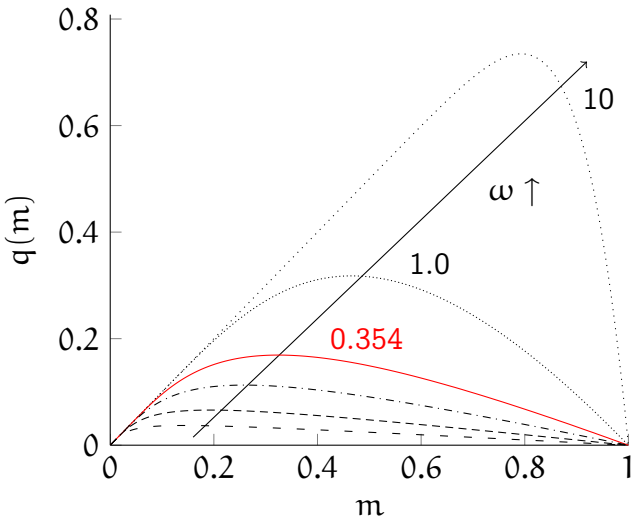

Figure 3: Normalized hydrodynamic cell flow as a function of cell occupation m for $\omega = \{0.05, 0.1, 0.2, 0.354, 1, 10\}$ and $a_\xi = 1$.

For an increasing value of ω, the hydrodynamic cell flow grows and

its maximum shifts to higher densities. Intuitively, this is due to the fact that for larger values of ω, the prevailing cell speed v decreases less with increasing density. The parameter ω can thus be interpreted as the sensitivity of walking speed to congestion, where a larger value of ω implies that speed is reduced less by high densities. In the following, ω is referred to as 'sensitivity to congestion'.

The normalized PedCTM is mainly useful to describe the internal dynamics of the model, for which the absolute values of the free-flow speed and the jam density do not need to be known. When a real situation is considered, the values of these quantities are obviously important, and the non-normalized formulation of PedCTM has to be applied.

4 Calibration

For a complete specification of PedCTM, the parameter set $Z = (v_f, \gamma, k_c, \alpha, \beta)$ needs to be known. In this section, Z is calibrated on pedestrian tracking data collected in a pedestrian underpass of Lausanne railway station, Switzerland. The goal is to find a model specification which is capable of realistically describing flows in public walking areas.

Pedestrian underpass West (PU West) in Gare de Lausanne has an area of approximately 685 m^2. During the busiest period in the morning peak hour between 100 and 400 pedestrians pass through it every minute. Figure 4 shows a layout of PU West. It connects the exterior of the train station to the five main platforms (platform 1, 3/4, 5/6, 7/8 and 9). There is a second underpass, PU East, which is however less used and does not provide access to all platforms (Hänseler et al., 2013). PU East is not considered in this study.

A state-of-the-art pedestrian tracking system composed of 32 visual, depth and infrared sensors allows to record hundreds of pedestrian trajectories simultaneously in PU West. The position of each pedestrian is tracked across space and time with a resolution of less than a meter and a few hundred milliseconds, respectively. A sparsity driven framework is used to segment foreground silhouettes given a dictionary of pre-computed ideal silhouettes (Alahi et al., 2011).

The maximum occupation in PU West can exceed 250 pedestrians in the morning peak hour. Sojourn times are typically in the range of 30

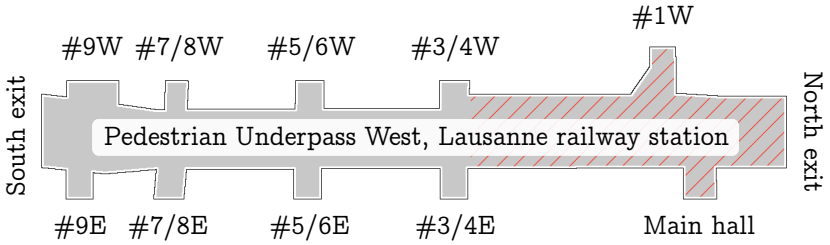

Figure 4: Pedestrian underpass West (PU West) in Lausanne railway station, Switzerland. It represents the busiest walking area in the railway station, connecting the exterior to train platforms. For calibration, the shaded area in the North part of PU West is used.

seconds to one minute. Mean density levels are generally below 1.3 m^{-2} (aggregation over 7.29 m^2 and 60 second periods, see also figure 16), but can locally and temporarily exceed this value.

For PedCTM, the area of PU West is discretized into 93 square cells of length $\Delta L = 2.7$ m. Cell size has been chosen based on geometrical considerations. The computation time step Δt depends through equation (2) on the cell length ΔL and the free-flow walking speed v_f, which is a calibration parameter. A potential influence of the space discretization on model dynamics has been investigated, but has been found negligible as long as the size of cell areas remains in the same order of magnitude. For the original cell transmission model, this invariance with respect to space discretization has been discussed theoretically (Daganzo, 1994).

For calibration, the north side of PU West (shaded area in figure 4) is considered. Pedestrian tracking data collected in the time period between 07:32 and 07:57 on April 9, 10, 18 and 30, 2013 is used for calibration. A further data set, collected on January 22 of the same year, will subsequently be employed for validation (section 6).

Travel time is assumed to build the basis for comparison between trajectory data and model prediction. Suppose that for each pedestrian group $\ell \in \mathcal{L}$, a measurement and a model prediction for average travel time, $\overline{TT}_\ell^{obs}$ and $\overline{TT}_\ell^{PedCTM}$, are available. If the squared error is used as distance measure, the objective function of the calibration problem can be expressed as

$$V(z) = \sum_{\ell \in \mathcal{L}} \left(\overline{TT}_\ell^{PedCTM}(z) - \overline{TT}_\ell^{obs} \right)^2 \tag{19}$$

and the optimal set of parameters is given by

$$z^* = \arg\min_z V(z). \tag{20}$$

Table 1 shows the parameter set z^* for each day obtained using simulated annealing (Kirkpatrick et al., 1983). It is assumed that the set of parameters is homogeneous across cells. Irrespective of initial conditions, the algorithm converged in most cases very closely to the reported values after a few hundred iterations.

Table 1: Results of the calibration runs of four different days. For comparison, values reported by Weidmann (1993) are shown.

	v_f	γ	k_c	α	β
April 9	1.20	1.50	4.42	2.44	0.005
April 10	1.30	1.74	5.83	1.99	0.012
April 18	1.22	1.95	5.88	2.08	2.55
April 30	1.30	1.87	4.83	1.86	0.169
Weidmann	1.34	1.913	5.4	–	–

It can be seen that the parameter values vary considerably across days. Nevertheless, all reported figures deviate less than 10% from the values reported by Weidmann (1993), except for April 9, where the deviation is slightly larger. The weight of the static floor field is estimated at between 1.86 and 2.44 (between 1.86 and 2.08 without April 9). The calibration does not yield an unambiguous estimate of the weight β, which is found in the range between 0.005 and 2.55.

To evaluate the parameter candidates presented in table 1, each of them is applied to all four days. Table 2 shows the results of this cross-validation. A similar approach has been followed by Johansson et al. (2007), whose efforts to calibrate the social force model have been mentioned in the introduction. They found that a broad range of parameter combinations performs almost equally well and applied a cross-validation on three data sets for choosing the optimal specification as well.

From table 2, it can be seen that the parameter set from the calibration run corresponding to April 9 leads to very high errors. An analysis has revealed that the low value of β is at the root of the large deviation.

Since pedestrians do not give preference to less busy cells, they repeatedly get stuck in a gridlock, leading to unrealistically high travel times. Such jams often arise in counter-flow situations near entrance areas. The other candidate sets lead to an increase of the prediction error of less than 15% as compared to the day-specific optimal parameter set. For the three parameter sets calibrated on April 10, 18 and 30 data, the error distribution is approximately normal.

Table 2: Cross-validation of the calibrated parameter candidates reported in table 1.

	$(V(z) - V(z^*))/V(z^*)$			
	$Z_{\text{April 9}}$	$Z_{\text{April 10}}$	$Z_{\text{April 18}}$	$Z_{\text{April 30}}$
April 9	0	9.8%	5.0%	8.0%
April 10	91.7%	0	2.4%	4.3%
April 18	100.2%	13.0%	0	13.0%
April 30	10^3	14.7%	3.7%	0

The increase in the prediction error in the cross-validation is smallest for the parameter set $Z_{\text{April 18}}$, for which it is no larger than 5%. Given its good performance, it will subsequently be used as default. From the values of the jam density, $k_c = 5.88\ \text{m}^{-2}$, and the shape parameter, $\gamma = 1.95\ \text{m}^{-2}$, a sensitivity to congestion of $\omega = 0.332$ results, which is relatively close to the value of 0.354 obtained for Weidmann's specification (Weidmann, 1993).

5 Model illustration and sensitivity analysis

To illustrate the behavior of PedCTM, several distinct flow patterns are studied (figure 5). This approach is inspired by Duives et al. (2013), who consider in total eight basic scenarios. Four of them, namely uni-directional (figure 5a), counter- (figure 5b), cross- (figure 5c) and corner-flow (figure 5d), are investigated analogically in this work. While they consider bottleneck entry- and exit-flows separately, here both cases are studied jointly (figure 5e). Two further flow patterns, a cross-flow involving more than two flows and general multidirectional flows, will be investigated subsequently in the framework of a real case study.

The first four scenarios are considered by means of a peak flow, i.e., the propagation of a single group of pedestrians is studied. The fifth flow pattern considers continuous flow of people over an extended period of time. Cells are assumed to be initially empty and of default size, i.e., $m(\xi, \tau = 0) = 0$ and $a_\xi = 1$, $\forall \xi \in \mathcal{X}$.

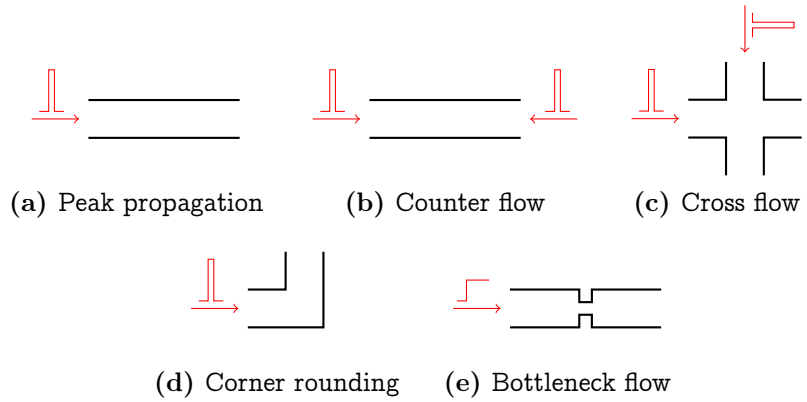

(a) Peak propagation **(b)** Counter flow **(c)** Cross flow

(d) Corner rounding **(e)** Bottleneck flow

Figure 5: Five generic flow scenarios illustrating the behavior of PedCTM under various conditions.

The propagation of a single pedestrian group along a homogeneous corridor represents the simplest of the flow scenarios studied in this work. Figure 6 shows a time-space diagram for a corridor with a length of 15 cells that is loaded at its left end with a pedestrian group of size $\chi_0 = 1$ (figure 5a; default parameters as defined in section 4 are used). White asterisks mark the cell with the highest density for each time step. It can be seen that the location of this density peak is located at the tail of the group throughout the movement. Furthermore, it is visible that the group disperses across time and space as intuitively expected.

By selectively perturbing the parameters of the default case, the influence of initial demand χ_0, sensitivity to congestion ω and weight α on peak propagation is investigated. For this purpose, the travel time of the previously identified density peak is considered. It represents a characteristic upper bound for travel times as can be seen from figure 6. Furthermore, the ratio of the peak and the minimum travel time, TT_{peak}/TT_{min}, can be interpreted as a measure of the spreading that occurs during the propagation.

In figure 7a, the influence of initial demand and sensitivity to congestion

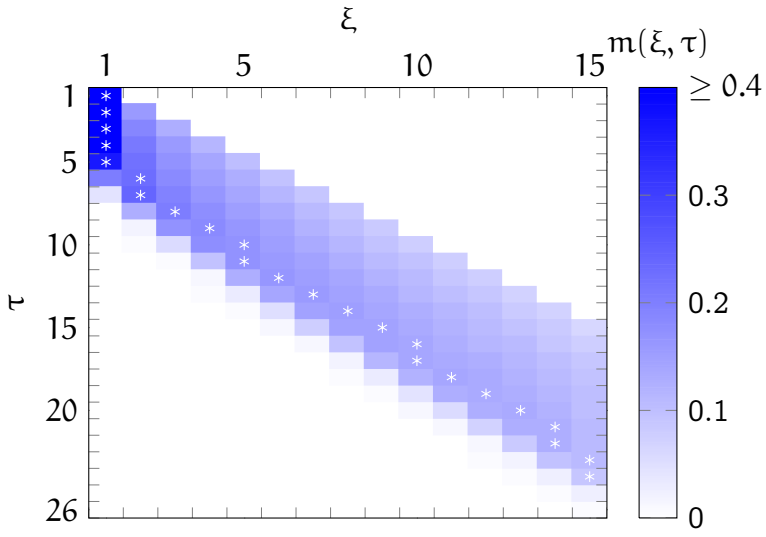

Figure 6: Time-space diagram of a pedestrian group propagating along a longitudinal corridor with a length of 15 cells. White asterisks mark for each time step the cell with the highest occupation, also referred to as the 'concentration peak' (Parameters: $x_0 = 1$, $\omega = 0.332$, $\alpha = 2.08$, $\beta = 2.55$).

on the peak travel time is shown. It can be seen that dispersion becomes more important with increasing demand, following approximately a linear relationship. The spreading is stronger for low values of ω, i.e., when the sensitivity to congestion is high. For low levels of demand, the peak travel time is equal to the minimum travel time irrespective of the choice of ω. These observations are again in good agreement with intuitive expectations.

The weight of the static floor field has a similar impact on the ratio TT_{peak}/TT_{min} as can be seen from figure 7b. At low values of α, pedestrians do not systematically walk towards the destination. This is why even for a small demand, the peak travel time TT_{peak} can be several times larger than TT_{min}. For small values of α, the spreading grows with increasing demand in a non-linear way, whereas for larger values of α, a linear increase in spreading is noticed. If α is set to zero, interestingly a moderate demand $x_0 \approx 1$ leads to the fastest propagation. Indeed, for $\alpha = 0$, pedestrians are solely driven by the dynamic floor field to leave the high density area built up around the inlet. For a very low demand, this effect is not significant. For a high demand, the additional delay incurred by congestion is prominent and leads to an increased spreading. Therefore, an accelerated

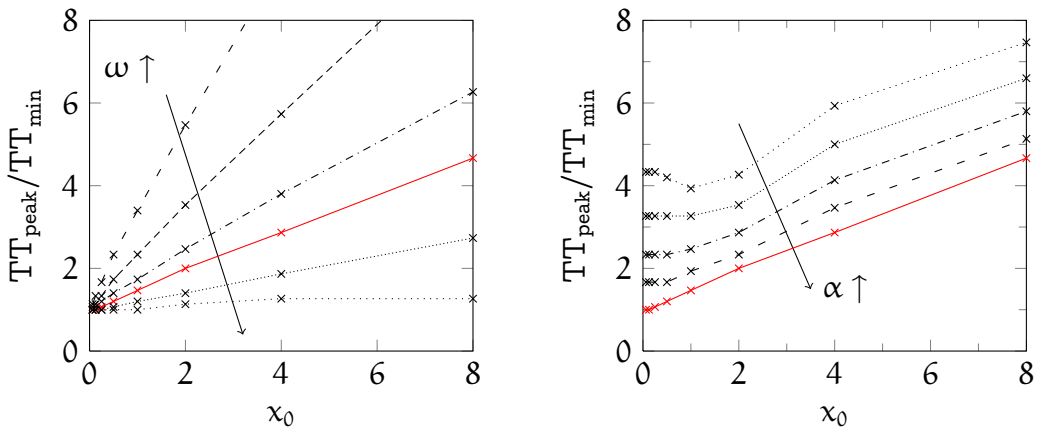

(a) $\alpha = 2.08$, $\omega = \{0.05, 0.1, 0.2, 0.332, 1, 10\}$ **(b)** $\alpha = \{0, 0.1, 0.25, 0.5, 2.08\}$, $\omega = 0.332$

Figure 7: Ratio of peak and minimum travel time as a function of the initial demand for different values of (a) sensitivity to congestion ω and (b) weight α. The curve in red represents the default case with $x_0 = 1$, $\alpha = 2.08$, $\beta = 2.55$ and $\omega = 0.322$.

propagation results only for $x_0 \approx 1$. No results for $\alpha > 2.08$ are shown, since the resulting curves almost coincide with the one obtained for default values.

Next, the interaction between two pedestrian groups propagating in opposite directions is investigated. This allows to study the superposition of two approaching waves of pedestrians, and more specifically the build-up and dissolution of congestion occurring when they overlap and separate, respectively. Figure 8 shows the time-space diagram of a corridor consisting of 15 cells in length, which is loaded at both ends with a pedestrian group of size $x_0 = 1$. Default parameters are assumed.

It can be seen that up to time step $\tau = 7$, the same pattern results as in figure 6. It follows a brief period of collision, during which both waves widen significantly. The post-collision distribution is therefore much more dispersed. For lower values of ω, the spreading both before and during the collision would be even stronger, leading to longer travel times and a flatter distribution (results not shown).

A similar case of bi-directional flow arises when two pedestrian groups meet at an orthogonal crossing. Such a situation is more complex as it involves en-route path choice. Figure 9 shows four snapshots representing the density pattern before, during, and after the collision in an orthogonal

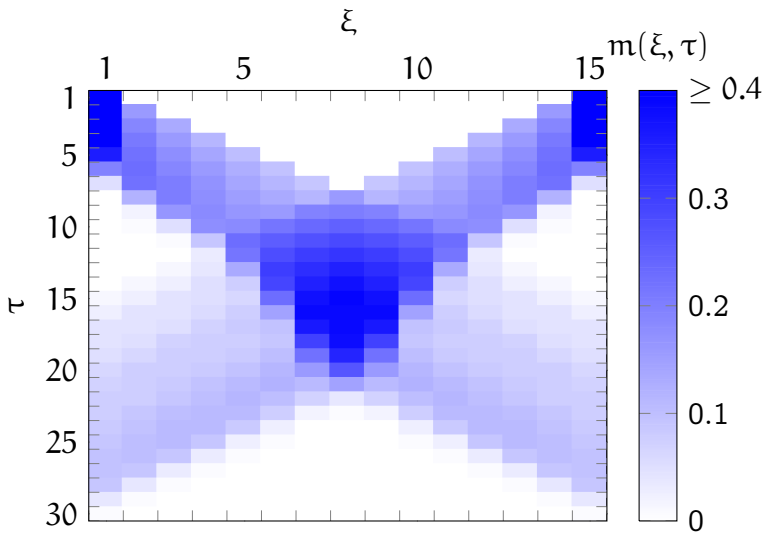

Figure 8: Time-space diagram of two colliding pedestrian waves in a homogeneous corridor with a length of 15 cells (Parameters: $x_0 = 1$, $\alpha = 2.08$, $\beta = 2.55$, $\omega = 0.332$).

cross-flow. Again an initial loading of $x_0 = 1$ for each flow and default parameters are assumed.

The maximum cell density is reached at the top left of the central part of the crossing during the time period $\tau = 10 \ldots 15$ (figure 9b and c). This time range starts significantly after the first contact between the two groups at $\tau = 4$. The reason is that the peak concentration of a group is found at its tail, as it has been observed previously.

To quantitatively investigate the influence of the weights α and β on the resulting flow pattern, the evolution of the cumulated arrivals η is investigated (figure 10). A semi-logarithmic scale allows to study their influence over a large range of time.

From figure 10a it can be seen that the propagation is accelerated with an increasing weight of the static floor field. This observation is based on a computation with $\beta = 2.55$, but similar findings hold for other values of β. It means that people reach their destination earlier if they follow the shortest path more strictly. For a simple cross-flow scenario, such a result is expected. It can however not be concluded that the same monotonic increase is found for more complex geometries, in particular if the scenario is such that a gridlock is likely to occur when everyone follows the shortest

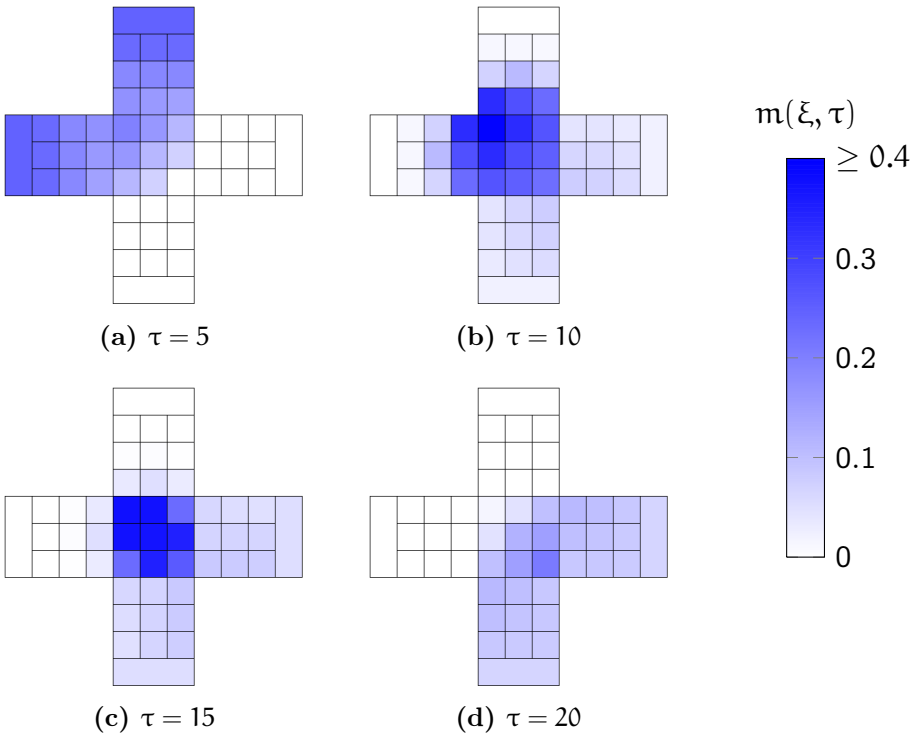

(a) $\tau = 5$ **(b)** $\tau = 10$ **(c)** $\tau = 15$ **(d)** $\tau = 20$

Figure 9: Density snapshots of a cross-flow scenario taken during four time intervals before, during and after the collision between two orthogonally moving pedestrian groups (Parameters: $\alpha = 2.08$, $\beta = 2.55$, $\omega = 0.332$, $x_0 = 1$).

path. Such a case has already been discussed in section 4.

In contrast, the influence of the weight β on the evolution of cumulated arrivals is not monotonic and generally smaller (figure 10b). For $\beta \leq 10$, only a small deviation from the reference case is observed. For large values of β, the cumulated arrivals grow less rapidly due to the large influence of congestion on local path choice.

As suggested by Duives et al. (2013), corner-flow is studied as a further basic flow pattern. Figure 11 shows three density snapshots of a corner-flow scenario obtained for default parameters and an initial demand $x_0 = 1$. As expected, a region of high density is formed upstream the corner, and pedestrians walk around it following a curved path. This resembles well the empirically observed 'corner rounding' (Duives et al., 2013).

So far, the model behavior has been investigated by analyzing the propagation of distinct pedestrian groups. To further elucidate the influence of

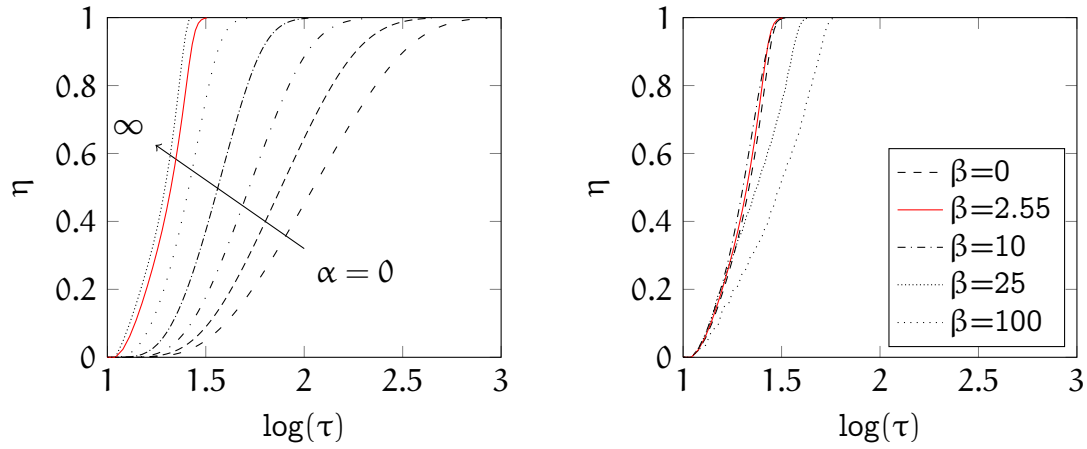

(a) $\alpha = \{0, 0.1, 0.25, 0.5, 1, 2.08, 100\}$, $\beta = 2.55$ **(b)** $\alpha = 2.08$, $\beta = \{0, 2.55, 10, 25, 250\}$

Figure 10: Cumulated arrivals as a function of time for different values of α (figure 10a) and β (figure 10b) for a cross-flow scenario (Parameters: $x_0 = 1$ and $\omega = 0.332$).

the static and dynamic floor fields on local route choice, a continuous flow through a bottleneck in a longitudinal corridor is studied. The corridor of interest has a length of 22 and a width of 6 cells. At the bottleneck, the width is reduced to two cells. During the first 100 time steps, a continuous inflow of $x = 1$ is imposed.

For different parameter values, figure 12 shows the density distribution arising 100 time steps after the continuous inflow is stopped, i.e., at $\tau = 200$. At this stage, pedestrians gradually propagate downstream, but the

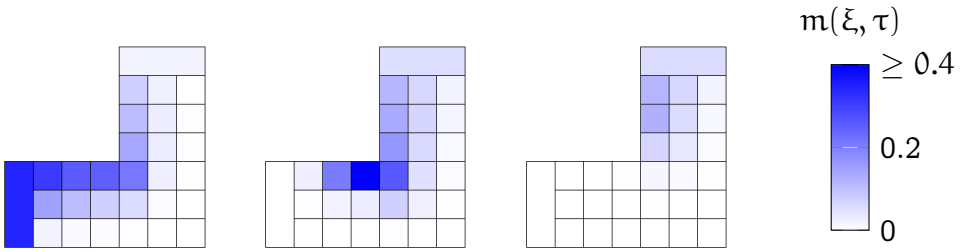

(a) $\tau = 8$ **(b)** $\tau = 16$ **(c)** $\tau = 24$

Figure 11: Density snapshots of a corner-flow scenario involving a single pedestrian group propagating through a bent channel of three cells width (Parameters: $\alpha = 2.08$, $\beta = 2.55$, $\omega = 0.332$, $x_0 = 1$).

dynamics of the model are relatively slow. The density pattern does not change fundamentally in the time range $\tau \approx 150 \ldots 250$ and is quasi non-transient.

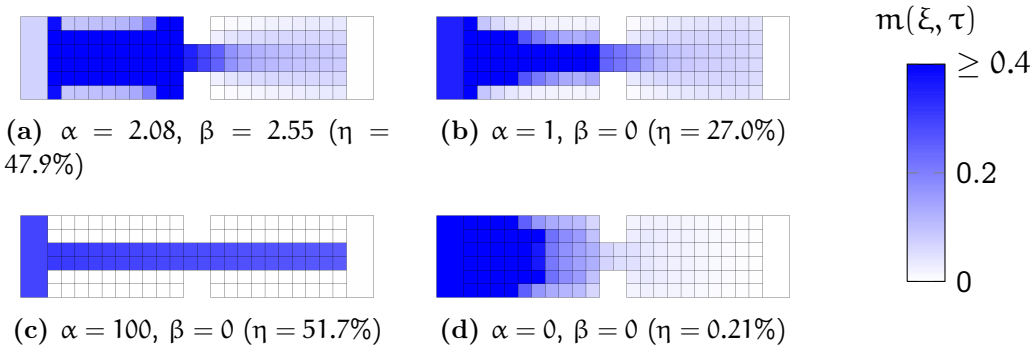

(a) $\alpha = 2.08$, $\beta = 2.55$ ($\eta = 47.9\%$)

(b) $\alpha = 1$, $\beta = 0$ ($\eta = 27.0\%$)

(c) $\alpha = 100$, $\beta = 0$ ($\eta = 51.7\%$)

(d) $\alpha = 0$, $\beta = 0$ ($\eta = 0.21\%$)

Figure 12: Flow patterns arising in a corridor with bottleneck for a continuous loading. During the first 100 time steps, a continuous inflow of magnitude $x = 1$ is imposed. Snapshots show the computed density field for time interval $\tau = 200$ for different values of α and β and a default sensitivity to congestion $\omega = 0.332$. The cumulated fraction of people having arrived at the destination $\eta(\tau = 200)$ is indicated in brackets.

The weights α and β have a significant influence on en-route path choice as can be seen from figure 12, in which a sensitivity to congestion of $\omega = 0.332$ has been assumed. Four specific choices of α and β are considered:

Figure 12a ($\alpha = 2.08$, $\beta = 2.55$, default case): Pedestrians take both the distance to destination and local flow conditions into account for local path choice. Upstream of the bottleneck, all space is occupied. People act as if they were impatient to pass the bottleneck, which is why a broad zone of high density builds up in front of the bottleneck. This behavior is well known from pedestrian facilities in railway stations (e.g. Daamen, 2004). This similarity is expected, as the used parameter set has been calibrated for precisely this scenario. At time step $\tau = 200$, 47.9% of all pedestrians have arrived at the destination. Besides everyday flows with very high demand, this pattern seems also realistic for an emergency situation where people are impatient to pass a bottleneck.

Figure 12b ($\alpha = 1$, $\beta = 0$): The density field shows that pedestrians walk along paths that 'anticipate' the bottleneck. Most, but not all space

is occupied. Less than a third of the population has reached the destination at $\tau = 200$. If pedestrians have a good queueing discipline, or if traffic is low, such a flow pattern seems accurate.

Figure 12c ($\alpha = 100$, $\beta = 0$)**:** People strictly follow the shortest path, irrespectively of flow conditions. Interestingly, this scenario yields the highest fraction of people having reached the destination at $\tau = 200$. This finding is to some extent analogous to the 'faster-is-slower' effect observed for evacuation by Helbing et al. (2000), who found that a lower desired velocity leads to a higher overall throughput. Here, it seems that a group of stoic pedestrians reaches its destination faster. This scenario represents an extreme case where pedestrians show a perfect queueing discipline or strictly minimize walking distance.

Figure 12d ($\alpha = 0$, $\beta = 0$)**:** When both weights are set to zero, the turning proportions of each group are completely homogeneous. This leads to a high density at the inlet and a very slow propagation. At $\tau = 200$, only $\eta = 0.22\%$ of all pedestrians have reached the downstream end. Such a situation might arise when people do not have any idea where to go, and do not have any preference with respect to congestion. If pedestrians give preference to less congested areas (e.g. $\alpha = 0$, $\beta = 1$), the flow pattern still strongly resembles figure 12d, but propagation is marginally faster. Neither of the two situations are very likely to be found in reality, but are reported for the sake of completeness.

To conclude, we found that when a dense group of pedestrians moves across space, its distribution gradually broadens over time. The peak concentration is located at the tail. If two groups of pedestrians interact, a high density results in the area of collision, and the groups disperse significantly. In an orthogonal layout with cross-flow, the highest densities are found in cells where the two groups meet first, however significantly after their first contact.

Three non-dimensional parameters have been identified that are key in describing the model dynamics. The sensitivity to congestion ω controls the way in which the mean walking velocity is affected by pedestrian density. A low value of ω implies that walking speed is significantly reduced with increasing density. This reduction in speed leads to dispersion and

consequently to longer travel times. The weights α and β parametrize the cell potential and thereby influence the en-route path choice. A large weight of the static floor field yields generally shorter travel times since pedestrians give a stronger preference to cells along the shortest path. The weight of the dynamic floor field governs the attitude of pedestrians towards prevailing traffic conditions. For increasing values of β, pedestrians are more willing to take a detour if it allows avoiding congested areas. This often leads to prolonged travel times, but can also be important in resolving gridlock situations.

While PedCTM is able to reproduce a wide range of behavioral patterns from panic situations to disciplined queueing, it is originally designed to describe everyday pedestrian flows in public spaces. Such a situation is discussed in the following section that provides a detailed case study analysis of Lausanne railway station.

6 Case study and validation

To assess the practical applicability of PedCTM, a detailed analysis of pedestrian flows in PU West of Lausanne railway station (see figure 4) is carried out. The period between 07:40 and 07:45 in the morning peak hour of January 22, 2013, serves as case study. It represents the busiest five-minute period throughout the day in Lausanne railway station. While for calibration only the North part of PU West has been considered, for validation the complete pedestrian underpass is analyzed.

The performance of PedCTM is evaluated in two ways with respect to predictions of travel times and density levels. First, its results are compared with the ground truth that is available from tracking data. Second, PedCTM is compared with Viswalk (PTV, 2013, Version 5.40) that implements the social force model (SFM; Helbing and Molnár, 1995). Introduced less than two decades ago, SFM is the current state of the art in pedestrian flow modeling.

For PedCTM, the default parameter set $Z_{\text{April 18}}$ is used, resulting in a simulation time step of length $\Delta t = \Delta L / v_f = 2.22$ s. The same aggregation of space as described in section 4 is applied. For the simulation using SFM, default parameters of Viswalk are used, which are based on a calibration performed by Johansson et al. (2007). Pedestrian demand is aggregated in

60-second periods for Viswalk due to the lack of a suitable mechanism for using a disaggregate origin-destination demand table as input. To account for stochasticity, five simulation runs are performed and the average is calculated. More runs are not necessary, since only aggregated output is reported, which shows little fluctuation across the various runs. For both PedCTM and SFM, the time period between 07:37 and 07:47 is computed, but only results for the period between 07:40 and 07:45 are reported in order to remove a bias of an initially empty system.

In PU West, the most frequented route during the considered time period is the one connecting the main hall of the train station to the exterior part of platform 3/4. Table 3 shows the corresponding travel times for the time period between 07:40 and 07:45. To allow for a comparison with the social force model, travel times are aggregated in periods of one minute.

Table 3: Travel times between the main hall of Lausanne railway station and the exterior part of platform 5/6 (#5/6 West) according to tracking data (TT_{obs}), the social force model (TT_{SFM}), and PedCTM (TT_{PedCTM}). The first two columns show overall demand (X_{tot}) and the demand along the route of interest (X_ρ). Data as observed on January 22, 2013.

	X_{tot}	X_ρ	TT_{obs}	TT_{SFM}	TT_{PedCTM}
07:40 – 07:41	118	12	37.5 ± 4.8	36.7 ± 2.2	48.0 ± 4.0
07:41 – 07:42	343	20	45.0 ± 5.4	68.1 ± 27.3	53.2 ± 7.1
07:42 – 07:43	251	10	50.9 ± 2.8	63.0 ± 18.2	50.7 ± 5.1
07:43 – 07:44	199	8	39.8 ± 5.1	48.0 ± 15.3	48.6 ± 4.2
07:44 – 07:45	107	7	45.2 ± 3.1	40.1 ± 5.3	47.8 ± 3.9

During the time period of interest, the total demand in PU West fluctuates between 107 and 343 incoming pedestrians per minute (table 3). Despite being the most frequented route, the corresponding fraction of pedestrians X_ρ/X_{tot} is mostly below 10 %. Observed average travel times vary between 37.5 and 50.9 s, i.e., over a range of 13.4 s.

According to PedCTM, the expected value of travel time varies between 47.8 and 53.2 s, representing a relatively narrow range compared to observed data. The social force model produces average travel times in the range between 36.7 and 68.1 s., which is larger than observed in the ground truth. Overall, table 3 shows that PedCTM is able to correctly predict the

order of magnitude of travel times. However, due to the high stochasticity present in the observed data, it is difficult to draw conclusions about its predictive power. A more aggregated validation of walking times seems worthwhile.

Figure 13a shows a histogram of group-specific travel times according to pedestrian tracking data and as computed by PedCTM. The bin size corresponds to the simulation time step of PedCTM, i.e., the lowest available level of aggregation. PedCTM slightly overestimates the frequency of travel times beyond 70 s, and underestimates the occurrence of short travel times below 20 s.

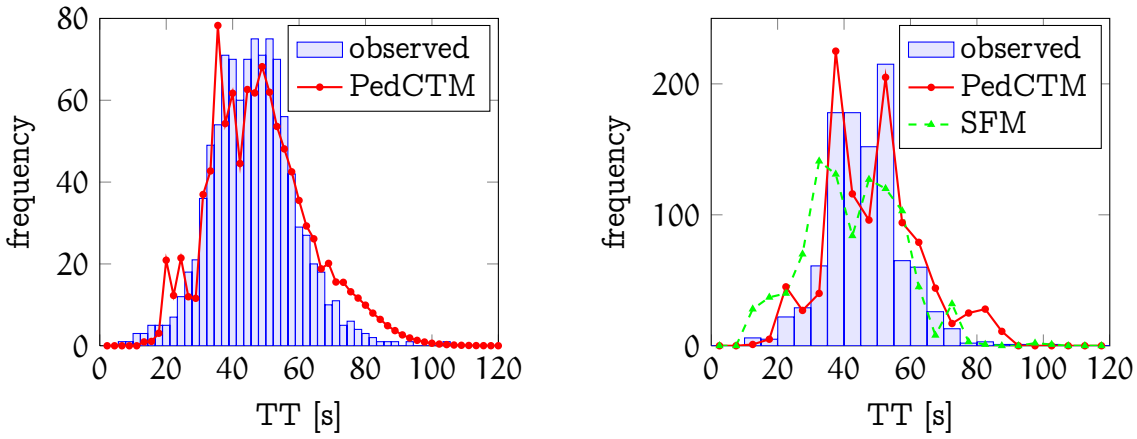

(a) Observed vs. PedCTM (aggregation period and diagram bin size equal to $\Delta t = 2.22$ s)

(b) Observed, SFM and PedCTM (aggregation over time period of 60 s, diagram bin size of 5 s)

Figure 13: Travel time distribution according to PedCTM, the social force model (SFM) and pedestrian tracking data.

To allow for a comparison with the social force model, figure 13b provides a similar comparison of route-specific travel times with a temporal aggregation of 60 s. The resulting mean values are shown in a histogram with a bin size of 5 s. As seen previously, PedCTM overestimates the occurrence of long travel times, but otherwise shows a reasonable agreement with trajectory data. The social force model seems to overestimate small travel times and to underestimate the most frequently observed travel times in the range between 35 and 55 s. Overall, the agreement between PedCTM and trajectory data is better than for SFM if the squared error is considered (114.4 vs. 181.6).

A comparison of the predicted and measured travel time distribution

for an individual route yields a similar result as for the overall distribution. Figure 14 shows the result for the busiest route, main hall to #5/6 West, that has already been investigated in table 3.

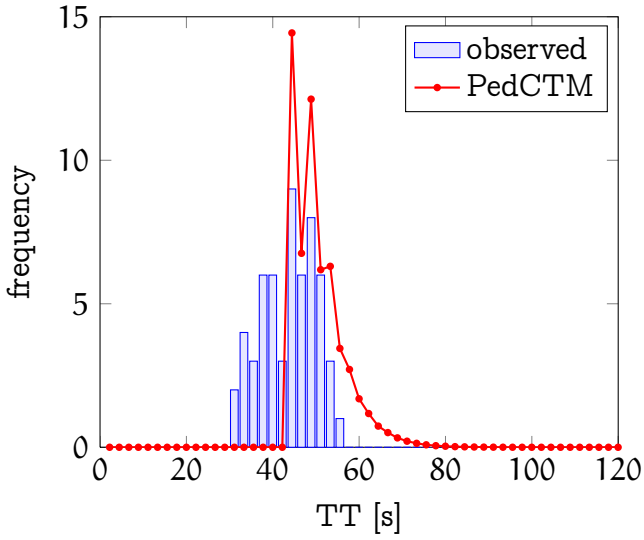

Figure 14: Travel time distribution corresponding to the busiest route in PU West in the time period between 7:40 – 7:45 on January 22, 2013 according to PedCTM and pedestrian tracking data.

PedCTM is unable to describe the 'faster' half of the travel time distribution, i.e., walking times that are shorter than the theoretical free-flow travel time. For instance, the shortest observed travel time for the route and time interval of interest amounts to 30.9 s, which corresponds to an average walking speed of 1.75 m/s. An analysis of other routes shows generally similar results, even though the mismatch between prediction and observation is mostly smaller.

Figure 15 shows the residuals of group-specific travel times computed using PedCTM compared to tracking data. The distribution of the absolute and the relative error is provided in figure 15a and 15b, respectively. In a first approximation, the histograms resemble a normal distribution with zero mean. From figure 15a, it can be seen that the predicted travel times deviate less than 10 s from the observed walking times for two thirds of the pedestrian groups. For less than 10% of all groups, the deviation is larger than 20 s. In relative terms, 50% of the estimates deviate less than 13% from observed values, and for more than 80% of all groups the relative error

is smaller than 33%. Also, it can be seen from the absolute residuals that there are a few particularly long walking times which cannot be reproduced by PedCTM at all.

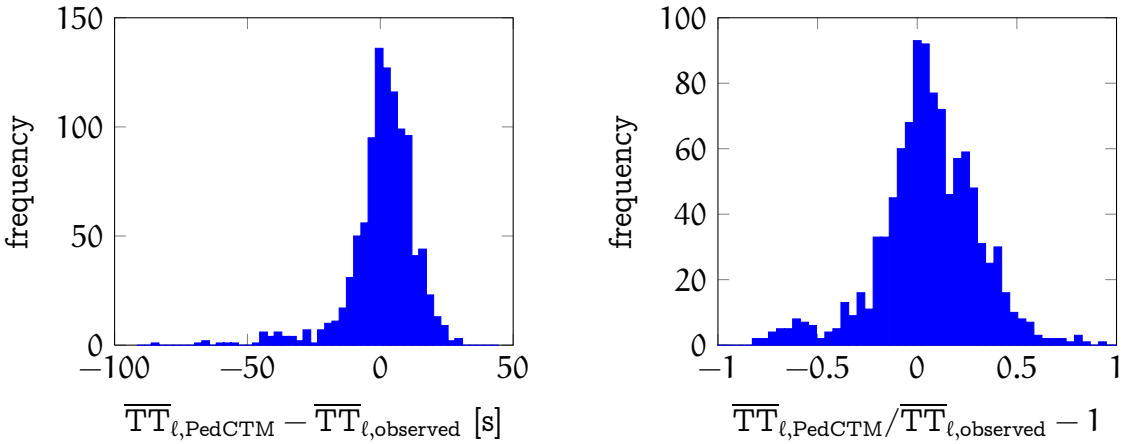

(a) Absolute error **(b)** Relative error

Figure 15: Absolute and relative residuals of travel time predictions by PedCTM for each pedestrian group ℓ, weighted by group size X_{ρ^ℓ,τ^ℓ}. Group-specific travel times are not readily available for the social force model from the used implementation and therefore not shown.

In conclusion, it can be noted that PedCTM is able to generate travel time predictions that are in reasonable agreement with observations. However, it underestimates very long travel times (see left tail of distribution in figure 15a). A reason for this discrepancy might be non-walking behavior of pedestrians, such as purchasing a ticket or checking the train timetable. These activities are not considered by the pedestrian walking model. Similarly, PedCTM fails at predicting very short travel times corresponding to average velocities that are higher than the free-flow speed. Both shortcomings are due to the assumption of a deterministic fundamental diagram, which associates with each density exactly one speed. In particular, it does not take into account that some pedestrians show walking speeds that are significantly higher than what is commonly acknowledged as free-flow speed in the literature. We believe that these limitations could be overcome by incorporating a stochastic fundamental diagram (Nikolic et al., 2013), which is subject to further research.

Besides walking times, density is an important indicator of level of service in pedestrian facilities. Figure 16 shows the density maps of PU West

as calculated from pedestrian tracking data, and as computed by the social force model and PedCTM. A discrete LOS scale ranging from A ('good') to F ('bad') is used for comparison (Highway Capacity Manual, 2000, Exhibit 18-3).

In the captions of figure 16, train arrivals relevant for each time interval are indicated. Train arrivals induce dense pedestrian waves that propagate through walking facilities and potentially lead to congestion. Both the social force model and PedCTM are able to reproduce the evolution of local pedestrian density relatively well. The highest pedestrian densities are observed between 7:41 and 7:43 due to various incoming trains. The level of service is in the range between A and E, i.e., densities are generally below 1.333 m^{-2}. Both PedCTM and SFM seem to underestimate the level of congestion during the peak minutes 07:41–07:44. According to the observed data, a region of high density forms along the center line of the corridor. In the two models, space is occupied more evenly, i.e., densities are overestimated laterally, and underestimated along the center line. During the time interval 07:42–07:43, SFM produces a gridlock situation in the narrow part of PU West. Specifically, pedestrians coming from North collide with pedestrians entering PU West from platform #5/6. As a consequence, locally a very high density exceeding 1.333 m^{-2} results (figure 16c) and travel times are significantly overestimated (table 3). This situation was observed in all five runs. In the ground truth, such a gridlock is not present. A detailed analysis shows that SFM is prone to predicting gridlocks also in other situations involving PU West (Hänseler et al., 2012). In contrast, PedCTM does not suffer from this shortcoming and thus seems better suited for infrastructure assessment in this particular case. In figure 16, PedCTM correctly predicts the local service level for 58.2% of all discretization cells, whereas for SFM an accuracy of 54.6% results.

Overall, despite the mentioned shortcomings, PedCTM is able to compute travel time distributions and density maps that are in agreement with observed data. In the case study considered above, it performed slightly better than SFM. Presumably, the performance of SFM can be improved by a dedicated calibration, but as it has been argued, this is a difficult task for disaggregate models. Thanks to its aggregate nature and the deterministic character, the computational cost of PedCTM is relatively low. A Java implementation of PedCTM without multi-threading is able to compute the above case study of PU West about ten times faster than Viswalk, a highly

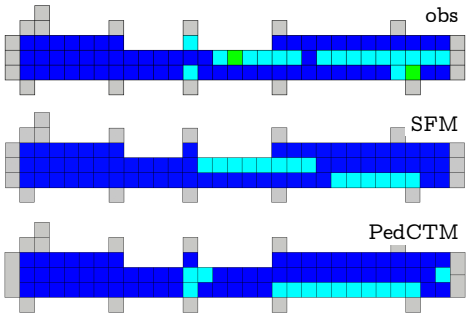

(a) 7:40–7:41: Relatively low occupation.

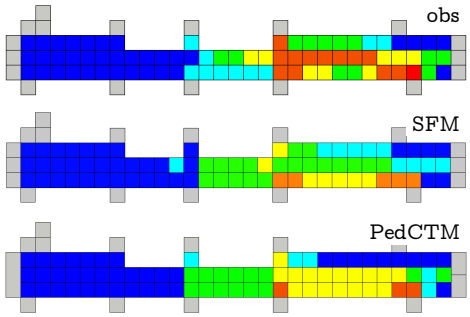

(b) 7:41–7:42: Arrival of train IR 1606 at 7:40:20 on platform 3/4.

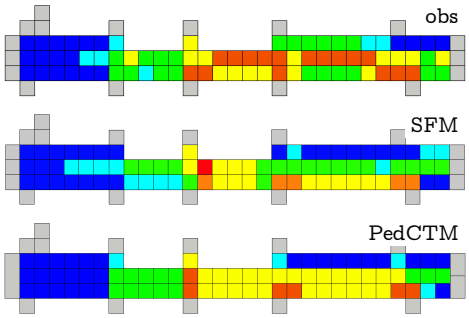

(c) 7:42–7:43: Arrival of train IR 706 at 7:41:24 on platform 5/6.

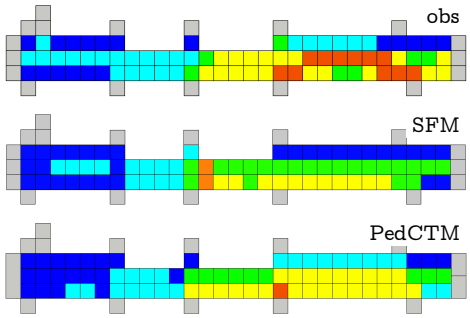

(d) 7:43–7:44: Arrival of train IR 1407 at 7:42:20 on platform 3/4.

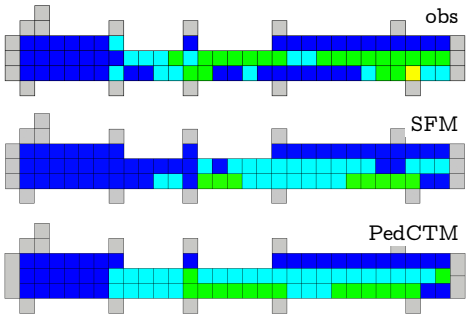

(e) 7:44–7:45: Gradual decrease in pedestrian occupation.

	LOS	Pedestrian density
	A	$k < 0.179$ [m^{-2}]
	B	$0.179 \leq k < 0.270$
	C	$0.270 \leq k < 0.455$
	D	$0.455 \leq k < 0.714$
	E	$0.714 \leq k < 1.333$
	F	$1.333 \leq k$

Figure 16: Pedestrian density map of PU West in Lausanne railway station for the time period between 7:40 and 7:45 on January 22, 2013. For each time period of one minute, the resulting maps obtained from pedestrian tracking data (obs), the social force model (SFM), and from PedCTM are shown. The color scale is as provided by NCHRP for pedestrian walkways (Highway Capacity Manual, 2000, Exhibit 18-3).

optimized implementation of the social force model.

7 Concluding remarks

In this work, we presented a novel framework for modeling pedestrians flows in transportation hubs and other public spaces. Such flows are typically multi-directional, non-stationary, and often congested during peak hours.

The proposed model considers space as a two-dimensional network of homogeneous cells. Each cell is part of a particular area, such as 'station hall' or 'train platform #1'. Most areas contain more than one cell, and sequences of connected areas form routes. Pedestrians are organized in groups, which are characterized by a route, a departure time interval, and a size.

To account for en-route path choice, a discrete choice model in combination with the concept of cell potentials is introduced. The cell potential consists of a static, route-specific component, and a dynamic, traffic-dependent part. Pedestrians are assumed to move in the direction of decreasing potential, i.e., they gradually propagate along their route, avoiding congested cells to the extent possible.

A modified cell-transmission model (CTM) is used to calculate flows between cells. For each pair of adjacent cells, group-specific sending capacities for the emitting cell, and a receiving capacity for the destination cell are computed. In absence of congestion, all sending capacities are accommodated. Otherwise, the receiving capacity is distributed following a demand-proportional supply scheme. This concept allows for studying the joint propagation of multiple pedestrian groups following different routes, assigning pedestrian flows in space, and better understanding phenomena such as congestion and dissolution of jams.

Our approach differs from related pedestrian propagation models in several aspects. First, its foundation on CTM allows for a realistic description of movement patterns under most flow conditions and at a relatively low cost. Compared to other CTM-based models, we use a dedicated fundamental diagram for pedestrian flows. Second, it provides a consistent modeling framework for multi-directional flows and local path choice. The model architecture allows to individually track the propagation of pedestrian groups across space and time. Third, the whole model is rigorously calibrated on

real pedestrian tracking data. The obtained model parameters are in good agreement with the literature.

Several properties of the presented model are explored by considering five generic test cases. First, the propagation of a pedestrian group along a corridor is investigated. Dispersion over time and space for different choices of parameters is discussed. It is shown that the peak concentration of a propagating pedestrian group is typically found at its tail. Furthermore, a counter and cross-flow scenario, corner rounding as well as a bottleneck flow are investigated. The influence of the cell potential on local path choice, and its impact on travel times are investigated in detail. Depending on the parametrization of the cell potential, the resulting flows resemble different behavioral patterns ranging from evacuation to patient queueing.

Subsequently, the model is applied to a real case study involving a pedestrian underpass in Lausanne railway station, Switzerland. A particularly busy five-minute period with over a thousand arriving pedestrians is considered. The model developed in this work is able to reproduce the overall travel time distribution and to generate realistic pedestrian density maps. However, it fails in predicting travel times corresponding to walking speeds that are faster than free-flow velocities as well as very slow travel times caused by non-walking behavior. Despite these shortcomings, a comparison with trajectory data and the social force model (Helbing and Molnár, 1995, SFM) shows a good performance of the developed model. Moreover, its computational cost is about one order of magnitude lower as compared to SFM.

To conclude, the proposed model provides an aggregate approach for studying large-scale problems of crowd dynamics in congested pedestrian facilities. It shows a realistic behavior due to its foundation on an empirical fundamental diagram and the performed systematic calibration. Due to its low computational requirements compared to disaggregate models such as the above mentioned social force model, it can be readily integrated in a real-time pedestrian flow simulator, considering dynamic demand estimation and assignment. Efforts along these lines are currently ongoing in our group. Furthermore, the use of a stochastic fundamental diagram is envisaged, as it likely will allow to explicitly model random fluctuations in walking time observed e.g. in the pedestrian tracking data presented in this work. In particular, this approach will allow considering different speeds for different classes of pedestrians such as ‘business travelers’, ‘commuters’,

'seniors', and so on.

Acknowledgement

Financial support by SNF grant #200021-141099 'Pedestrian dynamics: flows and behavior' as well as by SBB-CFF-FFS in the framework of 'Ped-Flux' is gratefully acknowledged.

References

Abdelghany, A., Abdelghany, K., Mahmassani, H. S., Al-Zahrani, A., 2012. Dynamic simulation assignment model for pedestrian movements in crowded networks. Transportation Research Record: Journal of the Transportation Research Board 2316 (1), 95–105.

Al-Gadhi, S. A., Mahmassani, H. S., 1991. Simulation of crowd behavior and movement: fundamental relations and application. Transportation Research Record 1320 (1320), 260–268.

Alahi, A., Jacques, L., Boursier, Y., Vandergheynst, P., 2011. Sparsity driven people localization with a heterogeneous network of cameras. Journal of Mathematical Imaging and Vision 41 (1-2), 39–58.

Antonini, G., 2005. A discrete choice modeling framework for pedestrian walking behavior with application to human tracking in video sequences. Faculty of Science and Technology in Engineering.

Asano, M., Sumalee, A., Kuwahara, M., Tanaka, S., 2007. Dynamic cell transmission-based pedestrian model with multidirectional flows and strategic route choices. Transportation Research Record: Journal of the Transportation Research Board 2039 (1), 42–49.

Ashok, K., Ben-Akiva, M. E., 2000. Alternative approaches for real-time estimation and prediction of time-dependent origin–destination flows. Transportation Science 34 (1), 21–36.

Ben-Akiva, M. E., Bierlaire, M., Burton, D., Koutsopoulos, H. N., Mishalani, R., 2001. Network state estimation and prediction for real-time traffic management. Networks and Spatial Economics 1 (3-4), 293–318.

Ben-Akiva, M. E., Lerman, S. R., 1985. Discrete choice analysis: theory and application to predict travel demand. Vol. 9. MIT Press.

Bierlaire, M., Crittin, F., 2006. Solving noisy, large-scale fixed-point problems and systems of nonlinear equations. Transportation Science 40 (1), 44–63.

Blue, V., Adler, J., 2001. Cellular automata microsimulation for modeling bi-directional pedestrian walkways. Transportation Research Part B: Methodological 35 (3), 293–312.

Cascetta, E., Inaudi, D., Marquis, G., 1993. Dynamic estimators of origin-destination matrices using traffic counts. Transportation Science 27 (4), 363–373.

Cascetta, E., Postorino, M. N., 2001. Fixed point approaches to the estimation of O/D matrices using traffic counts on congested networks. Transportation Science 35 (2), 134–147.

Çetın, N., 2005. Large-scale parallel graph-based simulations. Ph.D. thesis, ETH Zürich.

Charypar, D., 2008. Efficient algorithms for the microsimulation of travel behavior in very large scenarios. Ph.D. thesis, ETH Zürich.

Cheah, J. Y., Smith, J. M., 1994. Generalized M/G/c/c state dependent queueing models and pedestrian traffic flows. Queueing Systems 15 (1), 365–386.

Daamen, W., 2004. Modelling passenger flows in public transport facilities. Ph.D. thesis, Delft University of Technology.

Daganzo, C., 1994. The cell transmission model: A dynamic representation of highway traffic consistent with the hydrodynamic theory. Transportation Research Part B: Methodological 28 (4), 269–287.

Daganzo, C., 1995. The cell transmission model, Part II: Network traffic. Transportation Research Part B: Methodological 29 (2), 79–93.

Dijkstra, E. W., 1959. A note on two problems in connexion with graphs. Numerische mathematik 1 (1), 269–271.

Duives, D. C., Daamen, W., Hoogendoorn, S. P., 2013. State-of-the-art crowd motion simulation models. Transportation Research Part C: Emerging Technologies 37 (12), 193–209.

Guo, R., Huang, H., Wong, S., 2011. Collection, spillback, and dissipation in pedestrian evacuation: A network-based method. Transportation Research Part B: Methodological 45 (3), 490–506.

Hänseler, F., Molyneaux, N., Thémans, M., Bierlaire, M., 2013. Pedestrian strategies within railway stations: Analysis and modeling of pedestrian flows (PedFlux Mid-Term Report). Tech. rep., EPFL.

Hänseler, F., Sahaleh, S., Farooq, B., Lavadinho, S., Thémans, M., Bierlaire, M., 2012. Final report on the modeling part of the 'Flux piétons Gare de Lausanne' project within the framework of 'Léman 2030'. Tech. rep., EPFL.

Helbing, D., Farkas, I., Vicsek, T., 2000. Simulating dynamical features of escape panic. Nature 407 (487–490).

Helbing, D., Molnár, P., 1995. Social force model for pedestrian dynamics. Physical review E 51 (5), 4282–4286.

Highway Capacity Manual, 2000. Transportation Research Board. Washington, DC.

Hoogendoorn, S., Bovy, P., 2004. Pedestrian route-choice and activity scheduling theory and models. Transportation Research Part B: Methodological 38 (2), 169–190.

Hoogendoorn, S. P., Bovy, P. H., 2001. State-of-the-art of vehicular traffic flow modelling. Proceedings of the Institution of Mechanical Engineers, Part I: Journal of Systems and Control Engineering 215 (4), 283–303.

Hoogendoorn, S. P., Daamen, W., 2007. Microscopic calibration and validation of pedestrian models: Cross-comparison of models using experimental data. In: Traffic and Granular Flow'05. Springer, pp. 329–340.

Hughes, R. L., 2002. A continuum theory for the flow of pedestrians. Transportation Research Part B: Methodological 36 (6), 507–535.

Johansson, A., Helbing, D., Shukla, P. K., 2007. Specification of the social force pedestrian model by evolutionary adjustment to video tracking data. Advances in Complex Systems 10 (2), 271–288.

Kesting, A., 2012. Traffic Flow Dynamics: Data, Models and Simulation. Springer.

Kirkpatrick, S., Jr., D. G., Vecchi, M. P., 1983. Optimization by simmulated annealing. Science 220 (4598), 671–680.

Løvås, G. G., 1994. Modeling and simulation of pedestrian traffic flow. Transportation Research Part B: Methodological 28 (6), 429–443.

Mahmassani, H. S., 2001. Dynamic network traffic assignment and simulation methodology for advanced system management applications. Networks and Spatial Economics 1 (3-4), 267–292.

Nikolic, M., Bierlaire, M., Farooq, B., 2013. Spatial tessellations of pedestrian dynamics, 2nd Symposium of the European Association for Research in Transportation, September 05, 2013, Stockholm, Sweden.

Osorio, C., Bierlaire, M., 2009. An analytic finite capacity queueing network model capturing the propagation of congestion and blocking. European Journal of Operational Research 196 (3), 996–1007.

PTV, 2013. VISSIM 5.40 User Manual.
URL `http://vision-traffic.ptvgroup.com`

Rahman, K., Ghani, N. A., Kamil, A. A., Mustafa, A., Chowdhury, M. A. K., 2013. Modelling pedestrian travel time and the design of facilities: A queuing approach. PloS ONE 8 (5), e63503.

Robin, T., Antonini, G., Bierlaire, M., Cruz, J., 2009. Specification, estimation and validation of a pedestrian walking behavior model. Transportation Research Part B: Methodological 43 (1), 36–56.

Seyfried, A., Steffen, B., Klingsch, W., Boltes, M., 2005. The fundamental diagram of pedestrian movement revisited. Journal of Statistical Mechanics: Theory and Experiment 2005 (10), P10002.

Sherali, H. D., Park, T., 2001. Estimation of dynamic origin–destination trip tables for a general network. Transportation Research Part B: Methodological 35 (3), 217–235.

Weidmann, U., 1993. Transporttechnik der Fussgänger. Institute for Transport Planning and Systems, ETH Zürich.